Applied Surface Science 715 (2026) 164552

Contents lists available at ScienceDirect

Applied Surface Science

journal homepage: www.elsevier.com/locate/apsusc

Full Length Article

Driving sphere-to-rod transformation: How centrifugation-induced CTAB depletion reshapes gold nanoparticles

Min-Hsueh Tsai [a], Jyun-Hong Chen [a], Kun-De Lin [a], Chien-Hung Lin [b], Hsuan-Kai Lin [c], Sung-Po Chao [a], Jing-Yuan Ko [a], Jia-Ren Lee [a,*]

[a] Department of Physics, National Kaohsiung Normal University, Kaohsiung 824004, Taiwan
[b] Department of Physics, ROC Military Academy, Kaohsiung 830208, Taiwan
[c] Department of Materials Engineering, National Pingtung University of Science and Technology, Pingtung 912301, Taiwan

ARTICLE INFO

Keywords:
Gold nanoparticles
Centrifugation
Zeta potential

ABSTRACT

Centrifugation is conventionally regarded as a mere purification step in nanoparticle synthesis. Here, we challenge this view by demonstrating that centrifugation can be strategically employed as an active trigger to drive a predictable morphological transformation in gold nanoparticles (AuNPs). This study reveals a novel mechanism where repeated centrifugation systematically strips the cetyltrimethylammonium bromide (CTAB) stabilizer from the AuNP surface, inducing a controlled sphere-to-rod reshaping. We meticulously tracked this process: a dramatic drop in zeta potential from a stable + 46 mV to a highly unstable + 13 mV confirmed the loss of colloidal stability, while UV–vis spectroscopy captured the cycle-dependent emergence of a distinct longitudinal surface plasmon resonance (SPR) peak at 720 nm—a classic signature of nanorod formation. Direct transmission electron microscopy (TEM) imaging provided unequivocal visual evidence of the evolution from uniform spherical particles to well-defined nanorods. Moreover, this centrifugation-regulated reshaping provides an orthogonal, physically-driven approach to tuning anisotropy, which complements established chemical, optical, and electrochemical synthesis routes in applications ranging from surface-enhanced Raman spectroscopy to photothermal therapy. Our findings not only offer a deeper understanding of the interplay between mechanical forces and surface chemistry in nanoparticle systems but also open a new avenue for the rational design of anisotropic nanostructures, which serve as versatile platforms for biosensing. After appropriate surface functionalization to ensure biocompatibility, they also hold great promise for targeted therapies.

1. Introduction

The physical, chemical, and mechanical properties of materials [1,2], such as nanometals [3], nanoceramics [4], nanosemiconductors [5], and nanomagnetic materials [6] change notably due to the surface effect and quantum effect generated in the associated nanoscale phenomena. Among these materials, gold nanoparticles are a nanometal with unique optical, electrical, and catalytic properties [7,8], showing a significant potential in the fields of biomedicine [9–11] and environmental sciences [12–14]. Owing to the unique surface plasmon resonance (SPR) characteristics and high specific surface area, these nanoparticles exhibit excellent optical absorption capacity and reactivity; hence, they attract considerable attention in the fields of molecular detection and chemical reaction catalysis [15,16]. Moreover, these characteristics render gold nanoparticles potential candidates for achieving green chemical synthesis and energy conversion [17]. Because the properties of gold nanoparticles are highly dependent on their size and shape, researchers can optimize their properties by controlling the synthesis conditions. In common synthetic methods, CTAB is usually used as a stabilizer. It can form a double-layer structure around gold nanoparticles, effectively preventing nanoparticle agglomeration and stabilizing them in solutions [18]. Currently, gold nanoparticles have undergone rapid development for applications including disease diagnosis, drug delivery, antibacterial materials, and photothermal therapy [19]. Furthermore, their SPR characteristics endow them with great potential for bioimaging and therapeutic use.

While the role of CTAB in stabilizing gold nanoparticles is well-established, the post-synthesis purification process, particularly centrifugation, is often treated as a routine, passive step merely for removing excess reagents. The dynamic interplay between the mechanical forces

* Corresponding author at: Department of Physics, National Kaohsiung Normal University, Kaohsiung 82444, Taiwan.
E-mail address: kk22cc@mail.nknu.edu.tw (J.-R. Lee).

https://doi.org/10.1016/j.apsusc.2025.164552
Received 19 June 2025; Received in revised form 26 August 2025; Accepted 4 September 2025
Available online 5 September 2025

of centrifugation, the resulting depletion of surface stabilizers, and the consequential morphological evolution of nanoparticles remains an under-explored area. Most studies focus on preventing agglomeration, viewing it solely as an undesirable outcome that compromises nanoparticle function [20,21,22].

However, while CTAB is an effective stabilizer for synthesizing anisotropic gold nanoparticles, its inherent cytotoxicity poses a significant barrier to direct biomedical applications. The positive charge of CTAB can disrupt cell membranes and impair mitochondrial function, making CTAB-coated nanoparticles unsuitable for direct in vivo use. Therefore, for these nanostructures to be utilized in fields like drug delivery or phototherapy, a crucial post-synthesis step involving ligand exchange or surface coating with biocompatible materials is required to mitigate toxicity. In this context, our work focuses on establishing a novel physical method to control nanoparticle morphology, providing a versatile platform of nanostructures that can serve as precursors for biocompatible nanomaterials.

Here, we adopt a different perspective. We propose and demonstrate that centrifugation, far from being a simple purification tool, can be strategically utilized as an active and predictable trigger for the morphological reshaping of gold nanoparticles. This study systematically reveals how centrifugation-induced CTAB depletion drives a distinct sphere-to-rod transformation. By meticulously correlating changes in surface chemistry (zeta potential), optical properties (SPR), and morphology, as confirmed by transmission electron microscopy (TEM), we elucidate a controllable pathway to anisotropic nanostructures. This work reframes the understanding of nanoparticle agglomeration from a simple stability issue to a potential mechanism for post-synthesis morphological control, offering new insights into the rational design of functional nanomaterials for applications ranging from drug delivery [23,24] to high-sensitivity sensing [25,26].

2. Experiment

For the experimental solution preparation, a gold sheet and a platinum sheet were used as the anode and cathode, respectively. A total of 15 mL mixed solution was prepared by mixing cetyltrimethylammonium bromide (CTAB; $C_{19}H_{42}BrN$ (99.0 %); HSE Pure Chemicals, UK), which acts as the stabilizer, in deionized water (RODA analysis with an ultrapure water machine NDIT, water quality 18.25 MΩ). Subsequently, 90 μL acetone (C_3H_6O, 99.87 %, Chaneye Pure Chemical) was added to disperse the CTAB molecules. This solution was prepared in an ultrasonic oscillator (Elmasonic P30H) with a frequency of 37 kHz and a power of 120 W at a constant current of 2 mA for 10 min. All solutions were prepared in unbuffered deionized water, and the pH was not adjusted or monitored during the experiments. After preparation, the sample stock solution was aliquoted into centrifugal tubes and centrifuged for 20 min at 12,000 rpm (Hettich MIKRO 220, rotating radius: 87 mm). Following centrifugation, 970 μL of supernatant was pipetted from the centrifuge tube, leaving approximately 30 μL of the bottom fraction. Subsequently, 970 μL deionized water was added, and the contents were sonicated for 30 s to ensure thorough mixing. This sequence constitutes one centrifugation cycle. The experimental procedure was divided into two parts. The first part involved observing the yield and stability of gold nanoparticles prepared at CTAB concentrations of 0.07, 0.11, 0.13, 0.14, and 0.17 M (corresponding sample numbers are C007, C011, C013, C014, and C017). Then, samples prepared at a CTAB concentration of 0.11 M were centrifuged 1–3 times to drive and track the dynamic morphological evolution of gold nanoparticles caused by the detachment of CTAB molecules from the nanoparticle surface after centrifugation.

The absorption spectra of the prepared gold nanoparticle solution were measured using UV–vis spectroscopy (V-770, Jasco). The particle size distribution and zeta potential were determined using DLS (ELSZ-2000, Otsuka Electronics). TEM (JEM-1400, JEOL) was used to observe the surface morphology of nanoparticles. To ensure the reliability of our findings, the entire experimental process, from nanoparticle synthesis to multi-cycle centrifugation and characterization, was repeated with independently prepared batches of samples. The results presented in this study were found to be highly consistent and reproducible across these independent experiments. Due to the dynamically evolving nature of the system after centrifugation, reproducibility was assessed on a batch-to-batch basis rather than through repeated measurements on a single aliquot.

3. Results and Discussion

3.1. Analysis of absorption spectra and particle size

Fig. 1 shows the absorption spectra of samples prepared at different CTAB concentrations. Sample C011 exhibited the maximum absorbance, indicating the highest yield of nanoparticles. This suggests that 0.11 M is the optimal concentration for nanoparticle preparation under these conditions. The trend in peak absorbance for samples C013, C014, and C017 indicated that when the CTAB concentration exceeded 0.11 M, the generation efficiency of nanoparticles was notably reduced. According to previous reports [27–29], an increase in the surfactant concentration might inhibit electrochemical reactions, primarily because excess surfactant molecules can fully cover the metal surface, thereby inhibiting electron transfer and reaction. Although the absorbance values of these samples at spectral peaks were different, the spectral peak positions for samples C007, C011, C013, and C014 were almost the same, indicating that when the CTAB concentration in solutions reached a critical value, the nanoparticle surface would be covered with an adequate amount of CTAB molecules, maintaining the stability of nanoparticles. Even though the electrochemical reaction rates at various CTAB concentrations were different, the main particle sizes of generated nanoparticles were similar. Sample C017 exhibited unique behavior. Its absorbance was the lowest, conforming to the trend discussed above, but its spectral peak position showed a significant red shift compared to the other samples. This could be attributed to the effect of an excessively high CTAB concentration on the dispersion of components in the solution and the mobility and diffusion range of gold atoms. This would promote the generation of larger nanoparticles, contributing to absorption in the long-wavelength region and resulting in the observed red shift in the absorption spectrum.

Sample C011 was centrifuged 1–3 times to compare changes in the absorption spectra and particle size before and after centrifugation. As shown in Fig. 2 (a), the absorption spectra of gold nanoparticles exhibited peaks at 537 nm (before centrifugation), 535 nm (after 1st centrifugation), and 530 nm (after 2nd centrifugation), respectively.

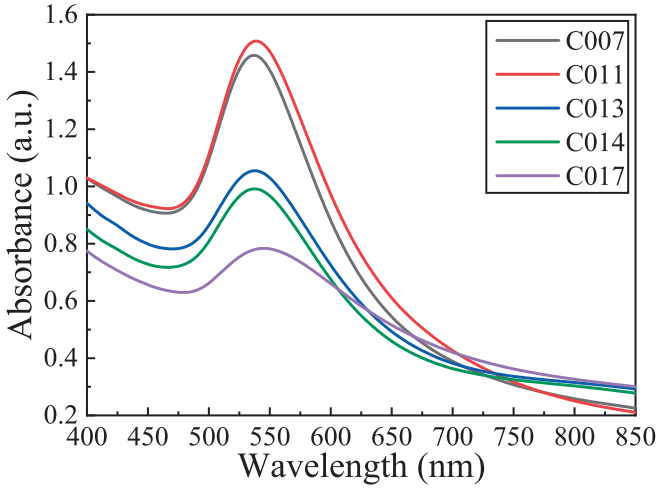

Fig. 1. Absorption spectra of samples with different CTAB concentrations.

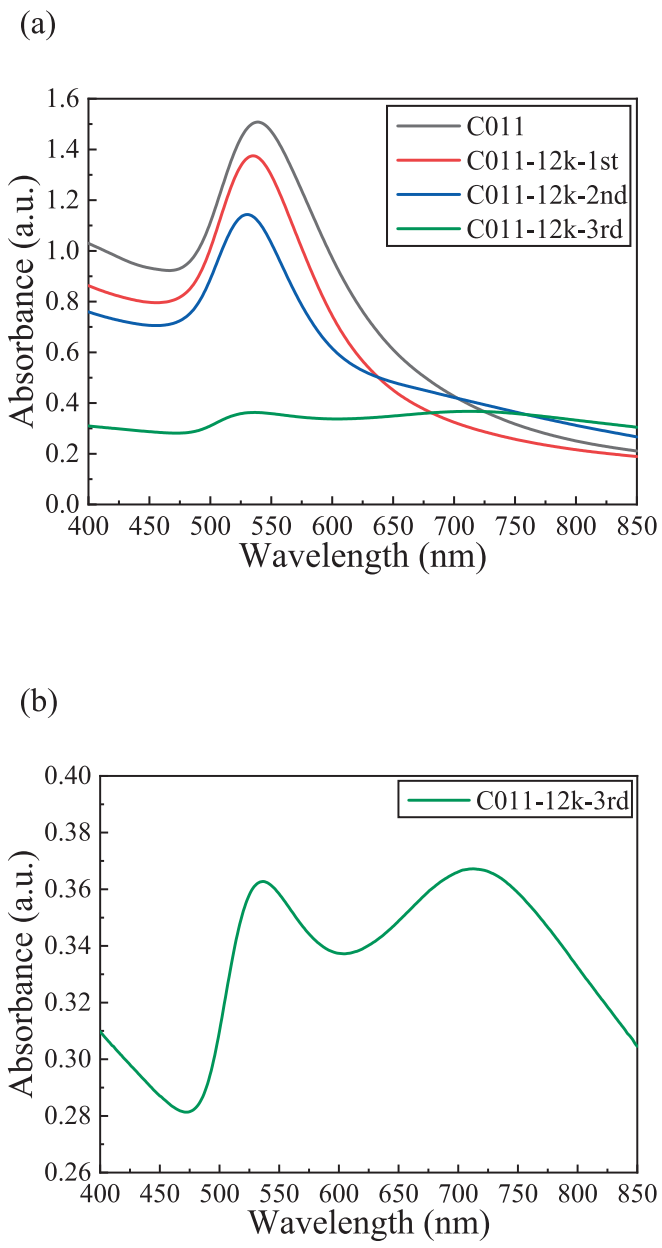

Fig. 2. Absorption spectra of sample C011: (a) before centrifugation and after the 1st, 2nd, and 3rd centrifugation cycles; (b) after the 3rd centrifugation cycle.

Furthermore, the peak absorbance decreased as the number of centrifugation cycles increased. This decrease is the initial optical signature of the onset of morphological transformation, driven by the depletion of isolated nanoparticles. As centrifugation systematically detaches CTAB molecules from the gold surface, the destabilized nanoparticles initiate a structural reconstruction to minimize their system energy, moving beyond simple settling. This process initiated the first stage of a structural reconstruction rather than simple particle settling, where the depletion of isolated nanoparticles led to the observed decrease in absorbance. Therefore, a decrease in absorbance is observed with an increasing number of centrifugation cycles. Fig. 2 (b) depicts the absorption spectra of the sample after the third centrifugation. In addition to the absorption peak at 536 nm, a peak with relatively high intensity appeared near 720 nm. This phenomenon signifies a remarkable reconstruction of nanoparticle morphology, actively triggered by the sharp decrease in CTAB concentration after multiple centrifugation cycles. This reconstruction involves the detachment of numerous CTAB molecules from the nanoparticle surface, allowing small nanoparticles in the solution to agglomerate into larger, reshaped structures, such as spherical nanoparticles or nanorods, which considerably increases the absorbance near 720 nm. The formation of these nanorods reflected the remarkable influence of the nanoparticle morphology on the optical properties, especially in the long wavelength region. After the second centrifugation, few nanorods were formed due to a significant decrease in the CTAB concentration, and absorbance near 720 nm tended to increase compared with those before centrifugation and after the first centrifugation, as shown in Fig. 2 (a). Fig. 3 shows the transmission light color of the gold nanoparticle solution before centrifugation and after the first, second, and third centrifugation. Owing to the CTAB depletion, the destabilized nanoparticles began to self-assemble to reduce their system energy. The resulting nanorods, formed via this directed attachment process, altered the solution's absorption band and intensity; consequently, the color of its transmission light changed considerably from magenta before centrifugation to purple after the third centrifugation, as shown in Fig. 3.

Fig. 4 displays an analysis diagram of the particle size and quantity of samples before and after repeated centrifugation. A key observation from these DLS results is the progressive decrease in the primary particle size, with the peak shifting from 27 nm (uncentrifuged) to 16 nm and 13 nm after the first and second cycles, respectively. This counterintuitive size reduction, occurring concurrently with nanorod formation, can be explained by two synergistic mechanisms driven by CTAB depletion.

Firstly, the centrifugation process leads to selective sedimentation, which preferentially removes the largest particles and any early-stage agglomerates from the supernatant being analyzed. Secondly, and more critically, the loss of the CTAB stabilizer induces a dissolution–recrystallization process. To minimize the high surface energy of the now-unstable system, smaller spherical nanoparticles partially dissolve, releasing gold atoms. These atoms then serve as the feedstock for anisotropic growth, recrystallizing onto the ends of the emerging nanorods.

This dual mechanism not only accounts for the observed size reduction in the remaining spherical population but also provides a clear chemical pathway for the material transport required for the sphere-to-rod transformation. This trend is highly consistent with the

Fig. 3. Transmission light color of gold nanoparticle solutions before centrifugation and after the first, second, and third centrifugation, shown from left to right.

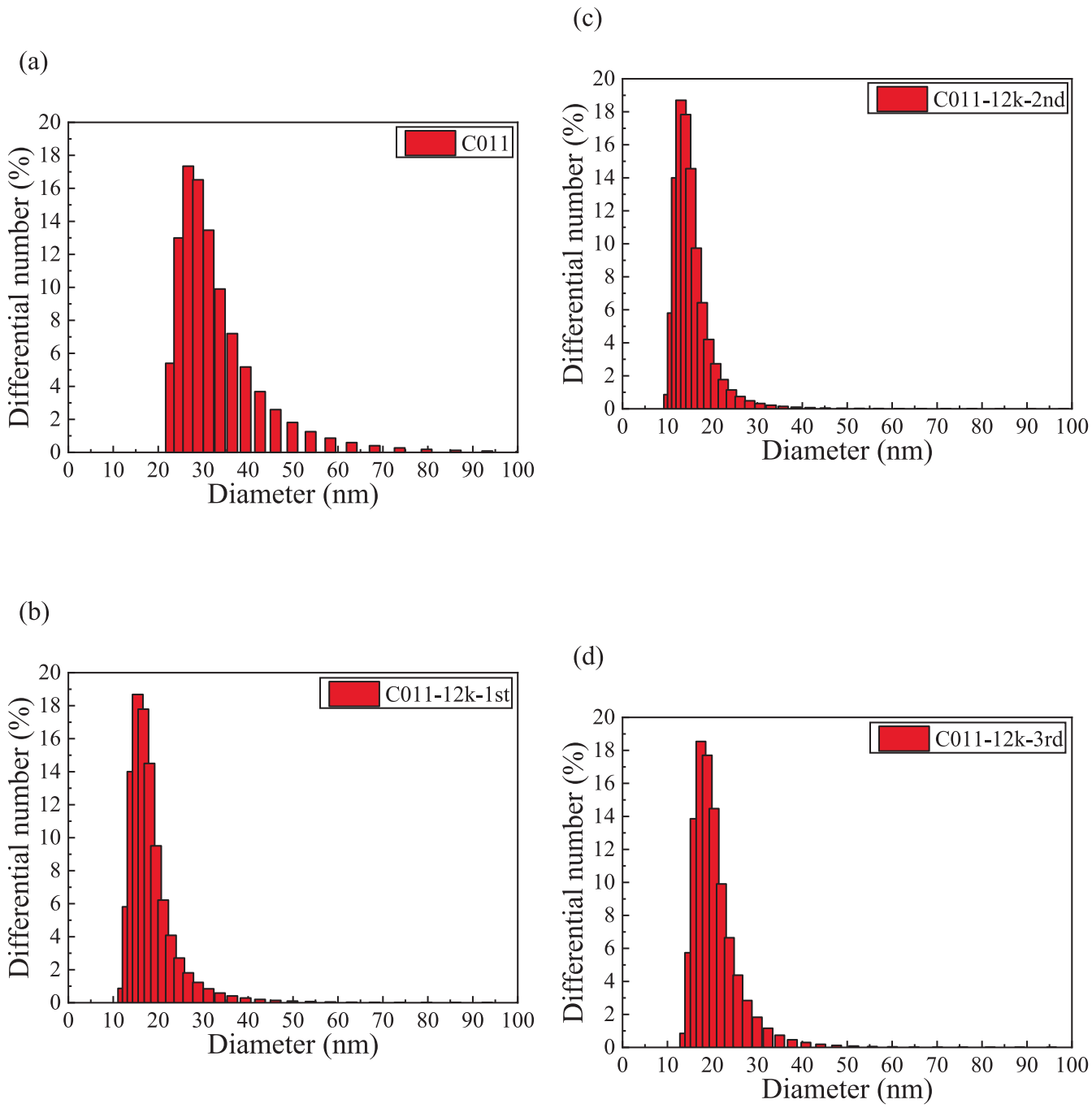

Fig. 4. Particle size distributions (by number) for sample C011: (a) before centrifugation; after the (b) 1st (c) 2nd and (d) 3rd centrifugation cycle.

corresponding blue shift in the primary spectral peak positions from 537 nm to 535 nm and 530 nm as observed in Fig. 2, which is characteristic of smaller spherical nanoparticles. Notably, after the third centrifugation, the primary particle size slightly increases to 18 nm, likely reflecting the growing contribution of the newly formed, larger nanostructures to the overall DLS signal.

As shown in Fig. 4 (d), although the sample centrifuged three times exhibited higher absorbance in the long wavelength region, no significant proportion of particles was observed at larger diameters in the number-weighted size distribution histogram. This observation might be attributed to discrepancies caused by the inherent differences in the DLS signals between gold nanorods and spherical nanoparticles during conversion into a number-based particle distribution. Gold nanorods exhibit distinct scattering patterns influenced by both translational and rotational diffusion, unlike the simpler translational diffusion of spheres. Because these conversion algorithms are based on spherical models (like Mie theory or Rayleigh approximation) to transform measured intensity autocorrelation functions into number distributions, they cannot adequately account for the anisotropy of nanorods. As a result, the quantity of nanorods is significantly underrepresented in the number-based results.

3.2. Zeta potential

Fig. 5 depicts the zeta potential measurement results of samples prepared with different CTAB concentrations. All five samples exhibited consistently high zeta potentials, ranging from 39 to 42 mV. These values signify that CTAB effectively imparted good stability to the

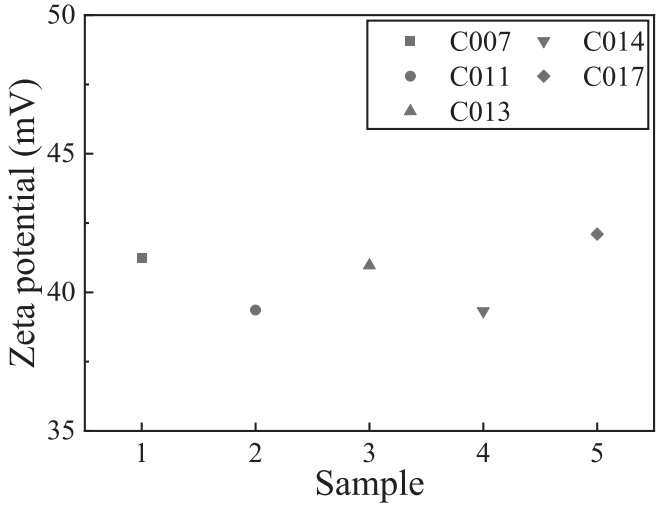

Fig. 5. Zeta potential of samples with different CTAB concentrations.

nanoparticles within the investigated concentration range. This finding is corroborated by the absorption spectra (Fig. 1), which showed distinct peaks characteristic of stable nanoparticle sizes. Taken together, these data indicate that adequate CTAB coverage within this concentration range resulted in a uniform surface charge. This uniform charge distribution is responsible for the high zeta potential values, which subsequently generate sufficient electrostatic repulsion to effectively prevent uncontrolled agglomeration.

As shown in Fig. 6, the zeta potential of sample C011 increased slightly after the first centrifugation compared with that before centrifugation. This means that the CTAB concentration in solutions was moderate and uniformly distributed after the first centrifugation, enabling more nanoparticles to be fully coated, thereby enhancing their zeta potential. However, after the second centrifugation, the zeta potential decreased from 46 mV to 21 mV due to the sharp decrease in the CTAB concentration in solutions [30,31,32]. Simultaneously, relatively unstable nanoparticles initiated a morphological evolution to reduce the system energy, corresponding to the results shown in Fig. 2 (a), where the sample centrifuged twice began to demonstrate an emerging peak in the long wavelength region. This phenomenon showed that when more CTAB was removed from solutions via centrifugation, CTAB molecules partially desorbed from the particle surfaces, leading to lower

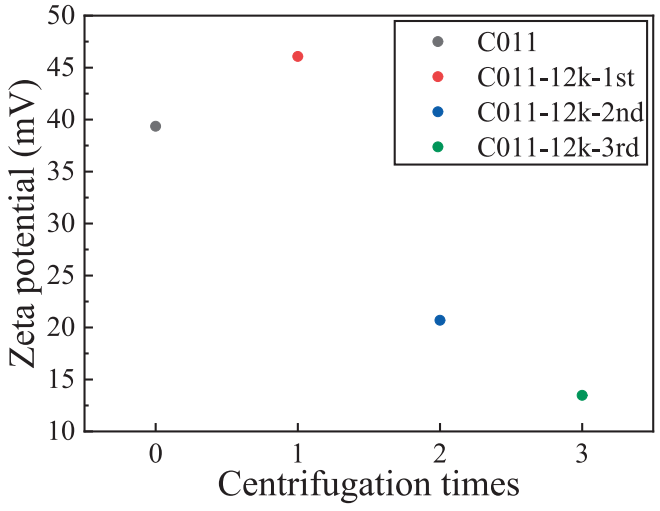

Fig. 6. Zeta potential of sample C011 before and after the first, second, and third centrifugation cycles.

electrostatic repulsion between particles and reduced stability. Following three centrifugation cycles, the zeta potential plummeted to + 13 mV. This value is well below the commonly accepted threshold for colloidal stability (typically $|\zeta| > 30$ mV), signifying that the system has entered a regime of extreme instability. While this may not represent the absolute final potential of a completely bare gold surface, it serves as the critical trigger point where the electrostatic repulsive forces are no longer sufficient to prevent nanoparticle aggregation and subsequent reorganization. This resulting instability is the primary driving force for the morphological evolution, leading to a marked increase in the population of nanorods within the solution as the system seeks a lower energy state. This also explains the considerable increase in the absorption intensity near 720 nm observed in Fig. 2 (b). When zeta potential decreased due to the gradual detachment of CTAB molecules, the electrostatic barrier effect between nanoparticles weakened, thereby promoting nanoparticle agglomeration. The change in zeta potential was consistent with the trend observed in the absorption spectra, confirming the correlation between the CTAB concentration and nanoparticle stability and further validating the important role of CTAB in maintaining the dispersion and stability of gold nanoparticles.

The regulatory mechanism revealed in this study holds potential for expanding the practical application scope of gold nanoparticles. For instance, while the as-synthesized nanorods are not directly suitable for in vivo applications, they can serve as excellent precursors for drug delivery systems after appropriate surface modification. The ability to precisely control the final morphology by regulating centrifugation steps could allow for the optimization of drug carrier characteristics. Once rendered biocompatible, gold nanorods are known to offer potentially higher drug loading capacities and better tissue penetration compared to their spherical counterparts, making them highly attractive for therapeutic applications. In addition, the regulatory mechanism of the CTAB concentration is helpful in developing a controlled release system, such as triggering CTAB detachment under a specific biological environment and inducing drug release. In terms of biosensing, the reshaping phenomenon induced by centrifugation can be utilized to regulate the optical properties of gold nanoparticles and to develop more sensitive surface-enhanced Raman scattering (SERS) sensors. In particular, gold nanorods formed during centrifugation can be used to prepare SERS substrates, remarkably enhancing the signal intensity and effectively enabling biomolecule and pathogen detections.

3.3. *Transmission electron microscopy (TEM)*

Fig. 7 displays the TEM image of sample C011 after the first, second, and third centrifugation. After the first centrifugation, the TEM results were consistent with the absorption spectra and zeta potential measurements; additionally, no agglomeration phenomenon was observed, and most gold nanoparticles had a particle size of 20–50 nm, as shown in Fig. 7 (a). This morphological evolution was quantified by analyzing the representative TEM images. As shown in Fig. 7(a), after the first centrifugation, the nanoparticles remained entirely spherical, with the nanorod population being 0 %. The onset of the transformation was observed after the second cycle (Fig. 7(b)), with a nascent nanorod population of approximately 1.5 %. Following the third centrifugation (Fig. 7(c)), the population of nanorods significantly increased to approximately 9 %.

This quantitative trend provides strong evidence for a threshold-dependent reshaping process. The transformation is initiated only after the second centrifugation, which is in excellent agreement with the sharp drop in zeta potential from + 46 mV to + 21 mV (Fig. 6) and the emergence of the longitudinal SPR peak in the UV–vis spectrum (Fig. 2a). This confirms that the morphological change is triggered once the CTAB depletion drives the system across a critical instability threshold.

A possible mechanism for the formation of nanorods and the evolution of spherical nanoparticles is illustrated in Fig. 8. This

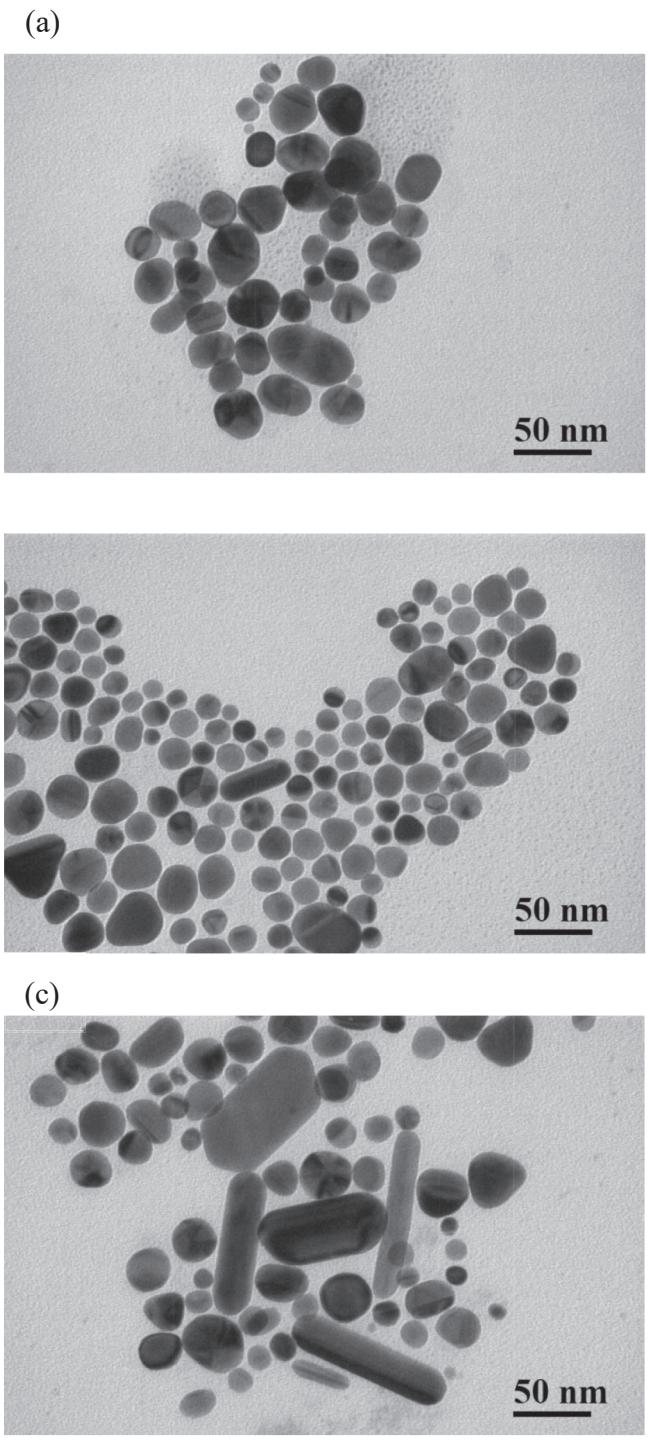

Fig. 7. TEM image of sample C011 after the (a) first, (b) second, and (c) third centrifugation. Based on analysis of these images, the nanorod population constitutes approximately 0%, 1.5%, and 9% of the total nanoparticles for each stage, respectively.

mechanically-driven reshaping occurs at a constant ambient temperature, with the process being triggered solely by the depletion of the CTAB stabilizer. Once destabilized, the nanoparticles initiate a directed attachment process. We hypothesize this occurs in several stages. First, the weakened electrostatic repulsion allows nanoparticles to overcome the energy barrier and collide. The attachment is non-random and likely guided by facet-selective interactions. This specificity is possibly due to residual CTAB molecules preferentially binding to certain crystallographic facets while leaving others with higher surface energy [33–35]. This directs the nanoparticles to align and attach along these specific high-energy interfaces.

Following attachment, the particles undergo crystallographic fusion and coalescence to eliminate the grain boundary and reduce the overall energy. This fusion and subsequent smoothing into a uniform rod structure is likely facilitated by a dissolution–recrystallization process. In this process, smaller, dissolving spherical particles provide the source of gold atoms. The continuous, one-dimensional repetition of this directed attachment and fusion sequence ultimately leads to the anisotropic growth of nanorods.

The SPR of gold nanorods oscillated in two directions: the short axis and long axis. Therefore, distinct resonance peaks corresponding to these axes can be observed in the visible and near-infrared regions [36]. As shown in Fig. 2, after sample C011 underwent a second centrifugation, its absorption spectrum began to exhibit an upward trend near 720 nm, compared to that after the first centrifugation. Fig. 7(b) also reveals that few nanorods were formed at this stage. Furthermore, after the third centrifugation, distinct absorption peaks appeared near both 536 and 720 nm. The TEM results provide compelling evidence that the formation of nanorods is responsible for the new absorption peak. As shown in Fig. 7(c), the population of nanorods is substantially higher after the third centrifugation than after the second. This clear increase in anisotropic particles provides compelling evidence that the pronounced absorbance peak at 720 nm is unequivocally attributed to the longitudinal surface plasmon resonance of the newly formed gold nanorods. The peak at 536 nm corresponds to their transverse resonance, as well as the resonance of any remaining spherical nanoparticles.

4. Conclusions

In conclusion, this study fundamentally challenges the conventional perception of centrifugation as a simple purification tool. We have successfully demonstrated that it can be repurposed as a strategic, active trigger for the post-synthesis morphological control of gold nanoparticles. By systematically depleting the surface-bound CTAB stabilizer, repeated centrifugation drives a predictable and controllable sphere-to-rod transformation. This mechanism was rigorously validated through a multi-faceted analysis, where the dramatic decrease in zeta potential, the emergence of a cycle-dependent longitudinal SPR peak, and direct TEM visualization of nanorod formation provided a cohesive and compelling body of evidence.

This work is significant in establishing a “centrifugation-regulated reshaping” methodology—a physically-driven, orthogonal control handle that complements existing chemical and optical synthesis routes for tuning nanoparticle anisotropy. Beyond deepening the fundamental understanding of the interplay between mechanical forces, surface chemistry, and nanoparticle evolution, this discovery provides a facile and novel approach for the rational design of anisotropic nanostructures. These structures are promising candidates for applications such as SERS, and after necessary surface modification to remove cytotoxic CTAB, for photothermal therapy and targeted drug delivery.

Building on this principle, future research can focus on several exciting directions. First and foremost, to further elucidate the atomic-scale details of the growth mechanism, advanced characterization techniques like high-resolution transmission electron microscopy (HRTEM) should be employed to directly visualize the lattice fusion during the directed attachment process. In addition, the effects of different surfactants on particle stability could be explored to identify stabilizers with greater biocompatibility that can either inhibit or controllably facilitate this reshaping [37,38]. The development of more accurate centrifugation technologies, such as gradient or continuous centrifugation, would also enable more precise control over the final nanoparticle size and morphology. With such advancements, the anisotropic nanorods produced via this method would be prime candidates for applications in biological imaging and treatment, leveraging

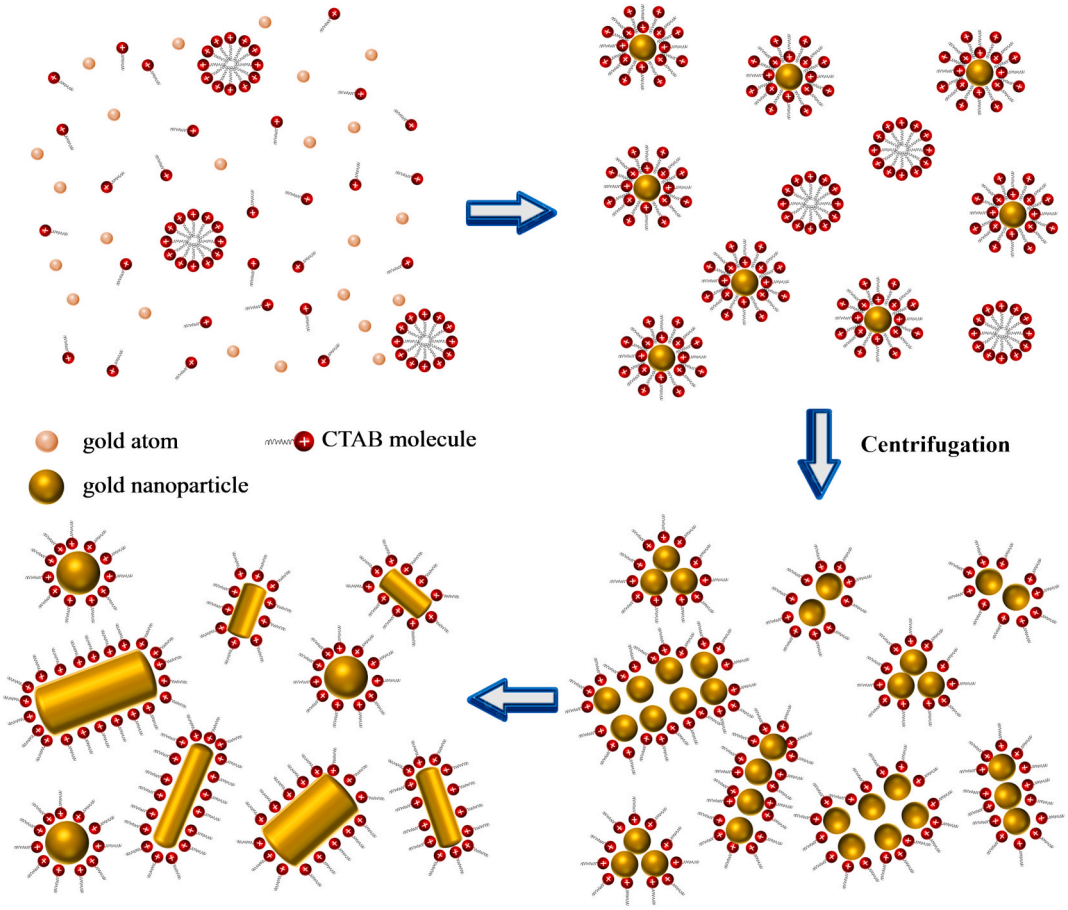

Fig. 8. Schematic of the formation of gold nanorods.

their unique photothermal effects and providing new opportunities for surface modification technologies. These research directions, grounded in the mechanism revealed herein, are crucial for advancing the application of nanotechnology in both biomedicine and environmental science.

CRediT authorship contribution statement

Min-Hsueh Tsai: Writing – original draft, Investigation. **Jyun-Hong Chen:** Writing – original draft, Investigation. **Kun-De Lin:** Writing – review & editing, Formal analysis. **Chien-Hung Lin:** Writing – review & editing, Formal analysis. **Hsuan-Kai Lin:** Writing – review & editing, Formal analysis. **Sung-Po Chao:** Writing – review & editing, Formal analysis. **Jing-Yuan Ko:** Writing – review & editing, Formal analysis. **Jia-Ren Lee:** Writing – review & editing, Investigation, Conceptualization.

Declaration of competing interest

The authors declare that they have no known competing financial interests or personal relationships that could have appeared to influence the work reported in this paper.

Acknowledgment

This work was supported by the National Science Council under grant numbers NSTC 112-2112-M-017-001 and NSTC 113-2112-M-017-001.

Data availability

Data will be made available on request.

References

[1] F.T. Rabouw, C. de Mello Donega, Excited-State Dynamics in Colloidal Semiconductor Nanocrystals, Top. Curr. Chem. (cham) 374 (5) (2016) 58, https://doi.org/10.1007/s41061-016-0060-0.
[2] B. Issa, I.M. Obaidat, B.A. Albiss, Y. Haik, Magnetic Nanoparticles: Surface Effects and Properties Related to Biomedicine applications, Int. J. Mol. Sci. 14 (11) (2013) 21266–21305, https://doi.org/10.3390/ijms141121266.
[3] L.M. Liz-Marzán, Nanometals: formation and color, in: Liz-Marzán L. (Ed.), Colloidal Synthesis of Plasmonic Nanometals, Jenny Stanford Publishing, 2020, pp. 1–13, https://doi.org/10.1201/9780429295188-1.
[4] A. Mukhopadhyay, B. Basu, Consolidation–Microstructure–Property Relationships in Bulk Nanoceramics and Ceramic Nanocomposites: a Review, Int. Mater. Rev. 52 (5) (2007) 257–288, https://doi.org/10.1179/174328007X160281.
[5] J. Liqiang, Q. Yichun, W. Baiqi, L. Shudan, J. Baojiang, Y. Libin, F. Wei, F. Honggang, S. Jiazhong, Review of Photoluminescence Performance of Nano-Sized Semiconductor Materials and its Relationships with Photocatalytic activity, Sol. Energy Mater. Sol. Cell 90 (12) (2006) 1773–1787, https://doi.org/10.1016/j.solmat.2005.11.007.
[6] M.E. McHenry, D.E. Laughlin, Nano-Scale Materials Development for Future magnetic applications, Acta Mater. 48 (1) (2000) 223–238, https://doi.org/10.1016/S1359-6454(99)00296-7.
[7] P.K. Jain, X. Huang, I.H. El-Sayed, M.A. El-Sayed, Review of some interesting Surface Plasmon Resonance-Enhanced Properties of Noble Metal Nanoparticles and their applications to Biosystems, Plasmonics 2 (3) (2007) 107–118, https://doi.org/10.1007/s11468-007-9031-1.
[8] P. Banerjee, D. Conklin, S. Nanayakkara, T.-H. Park, M.J. Therien, D.A. Bonnell, Plasmon-Induced Electrical Conduction in Molecular Devices, ACS Nano 4 (2) (2010) 1019–1025, https://doi.org/10.1021/nn901148m.
[9] J. Fokkema, J. Fermie, N. Liv, D.J. van den Heuvel, T.O.M. Konings, G.A. Blab, A. Meijerink, J. Klumperman, H.C. Gerritsen, Fluorescently Labelled Silica Coated Gold Nanoparticles as Fiducial Markers for Correlative Light and Electron Microscopy, Sci. Rep. 8 (1) (2018) 13625, https://doi.org/10.1038/s41598-018-31836-1.

[10] S.J. Hurst, A.K.R. Lytton-Jean, C.A. Mirkin, Maximizing DNA Loading on a Range of Gold Nanoparticle Sizes, Anal. Chem. 78 (24) (2006) 8313–8318, https://doi.org/10.1021/ac0613582.
[11] M.R.K. Ali, Y. Wu, M.A. El-Sayed, Gold-Nanoparticle-Assisted Plasmonic Photothermal Therapy advances Toward Clinical Application, J. Phys. Chem. C 123 (25) (2019) 15375–15393, https://doi.org/10.1021/acs.jpcc.9b01961.
[12] P. Nath, N. Priyadarshni, S. Mandal, P. Singh, R.K. Arun, N. Chanda, Gold nanostructure in sensor technology: Detection and estimation of chemical pollutants, in: S. Bhattacharya, A.K. Agarwal, N. Chanda, A. Pandey, A.K. Sen (Eds.), Environmental, Chemical and Medical Sensors, Springer, Singapore, 2018, pp. 31–66, https://doi.org/10.1007/978-981-10-7751-7_3.
[13] H. Chen, F. Wang, S. Xue, Novel Biosynthetic Aunps as the Efficient Catalyst for Organic Contaminants Degradation: One-step Preparation, Degradation Kinetics and Mechanism, Res. Chem. Intermed. 49 (7) (2023) 3045–3063, https://doi.org/10.1007/s11164-023-05026-2.
[14] B. Kumar, Green Synthesis of Gold, silver, and Iron Nanoparticles for the Degradation of Organic Pollutants in Wastewater, J. Compos. Sci. 5 (8) (2021) 219, https://doi.org/10.3390/jcs5080219.
[15] K. Xia, T. Yatabe, K. Yonesato, S. Kikkawa, S. Yamazoe, A. Nakata, R. Ishikawa, N. Shibata, Y. Ikuhara, K. Yamaguchi, K. Suzuki, Ultra-Stable and Highly Reactive Colloidal Gold Nanoparticle Catalysts Protected using Multi-dentate Metal Oxide Nanoclusters, Nat. Commun. 15 (1) (2024) 851, https://doi.org/10.1038/s41467-024-45066-9.
[16] H. Daraee, A. Eatemadi, E. Abbasi, S. Fekri Aval, M. Kouhi, A. Akbarzadeh, Application of Gold Nanoparticles in Biomedical and Drug delivery, Artif. Cells Nanomed. Biotechnol. 44 (1) (2016) 410–422, https://doi.org/10.3109/21691401.2014.955107.
[17] A. Carone, S. Emilsson, P. Mariani, A. Désert, S. Parola, Gold Nanoparticle Shape Dependence of Colloidal Stability Domains, Nanoscale Adv. 5 (7) (2023) 2017–2026, https://doi.org/10.1039/d2na00809b.
[18] A. Bano, A. Dawood, S. Rida, F. Saira, A. Malik, M. Alkholief, H. Ahmad, M. A. Khan, Z. Ahmad, O. Bazighifan, Enhancing Catalytic activity of Gold Nanoparticles in a Standard Redox Reaction by investigating the Impact of Aunps size, Temperature and Reductant Concentrations, Sci. Rep. 13 (1) (2023) 12359, https://doi.org/10.1038/s41598-023-38234-2.
[19] X. Huang, P.K. Jain, I.H. El-Sayed, M.A. El-Sayed, Plasmonic Photothermal Therapy (PPTT) using Gold Nanoparticles, Laser. Med. Sci. 23 (3) (2008) 217–228, https://doi.org/10.1007/s10103-007-0470-x.
[20] S. Basu, S.K. Ghosh, S. Kundu, S. Panigrahi, S. Praharaj, S. Pande, S. Jana, T. Pal, Biomolecule Induced Nanoparticle Aggregation: effect of Particle size on Interparticle Coupling, J. Colloid Interface Sci. 313 (2) (2007) 724–734, https://doi.org/10.1016/j.jcis.2007.04.069.
[21] I. Blakey, Z. Merican, K.J. Thurecht, A Method for Controlling the Aggregation of Gold Nanoparticles: Tuning of Optical and Spectroscopic Properties, Langmuir 29 (26) (2013) 8266–8274, https://doi.org/10.1021/la401361u.
[22] Y. Cao, X. Chen, M. Gu, Y. Zhang, Dynamically Engineering the Plasmonic Resonance of Gold Nanoparticles Fabricated through a Facile Annealing Process. In *Dynamically Engineering the Plasmonic Resonance of Gold Nanoparticles Fabricated through a Facile Annealing Process*, Elsevier BV (2024), https://doi.org/10.2139/ssrn.4820146.
[23] Y. Zhang, D. Xu, W. Li, J. Yu, Y. Chen, Effect of size, Shape, and Surface Modification on Cytotoxicity of Gold Nanoparticles to Human Hep-2 and Canine MDCK Cells, J. Nanomater. 2012 (1) (2012) 375496, https://doi.org/10.1155/2012/375496.
[24] R. Venkatesan, A. Pichaimani, K. Hari, P.K. Balasubramanian, J. Kulandaivel, K. Premkumar, Doxorubicin Conjugated Gold Nanorods: a Sustained Drug delivery Carrier for improved Anticancer Therapy, J. Mater. Chem. B 1 (7) (2013) 1010–1018, https://doi.org/10.1039/c2tb00078d.
[25] J. Najeeb, U. Farwa, F. Ishaque, H. Munir, A. Rahdar, M.F. Nazar, M.N. Zafar, Surfactant Stabilized Gold Nanomaterials for Environmental Sensing applications – a Review, Environ. Res. 208 (2022) 112644, https://doi.org/10.1016/j.envres.2021.112644.
[26] T. Li, Y. Li, Y. Zhang, C. Dong, Z. Shen, A. Wu, A Colorimetric Nitrite Detection System with Excellent Selectivity and High Sensitivity based on Ag@Au Nanoparticles, Analyst 140 (4) (2015) 1076–1081, https://doi.org/10.1039/c4an01583e.
[27] M.V. Shepida, M.A. Sozanskyi, Y.V. Sukhatskiy, A.S. Mazur, O.İ. Kuntyi, Sonoelectrochemical Synthesis of Silver Nanoparticles in Polyvinylpyrrolidone Solutions, CTAS 4 (1) (2021) 82–87, https://doi.org/10.23939/ctas2021.01.082.
[28] C. Li, W. Yang, W. He, X. Zhang, J. Zhu, Multifunctional Surfactants for Synthesizing High-Performance Energy Storage Materials, Energy Storage Mater. 43 (2021) 1–19, https://doi.org/10.1016/j.ensm.2021.08.033.
[29] M.A. Migahed, E.M.S. Azzam, S.M.I. Morsy, Electrochemical Behaviour of Carbon Steel in Acid Chloride solution in the Presence of Dodecyl Cysteine Hydrochloride Self-Assembled on Gold Nanoparticles, Corros. Sci. 51 (8) (2009) 1636–1644, https://doi.org/10.1016/j.corsci.2009.04.010.
[30] V. Zani, C. Renero-Lecuna, D. Jimenez de Aberasturi, D. di Silvio, S. Kavak, S. Bals, R. Signorini, L.M. Liz-Marzán, Core–Shell Colloidal Nanocomposites for Local Temperature monitoring during Photothermal heating, J. Phys. Chem. C 128 (41) (2024) 17787–17796, https://doi.org/10.1021/acs.jpcc.4c05593.
[31] A. Pedrazo-Tardajos, N. Claes, D. Wang, A. Sánchez-Iglesias, P. Nandi, K. Jenkinson, R. De Meyer, L.M. Liz-Marzán, S. Bals, Direct Visualization of Ligands on Gold Nanoparticles in a Liquid Environment, Nat. Chem. 16 (8) (2024) 1278–1285, https://doi.org/10.1038/s41557-024-01574-1.
[32] Y. Li, C. Jiang, Y. Zhou, H. Liu, Y. Zhang, Robust Encoding of Precise addressing Information on AUNPS to Direct their Heritable Positioning on DNA Origami†, Chin. J. Chem . 43 (5) (2025) 548–552, https://doi.org/10.1002/cjoc.202400957.
[33] J. Xiao, L. Qi, Surfactant-Assisted, Shape-Controlled Synthesis of Gold Nanocrystals, Nanoscale 3 (4) (2011) 1383–1396, https://doi.org/10.1039/c0nr00814a.
[34] M.A. Matin, H. Kim, J.K. Saha, Z. Zhang, J. Kim, J. Jang, Monte Carlo Study on the Self-Assembly of Nanoparticles into a Nanorod Structure, J. Nanosci. Nanotechnol. 13 (9) (2013) 6254–6258, https://doi.org/10.1166/jnn.2013.7684.
[35] J.-Y. Kim, M.-G. Han, M.-B. Lien, S. Magonov, Y. Zhu, H. George, T.B. Norris, N. A. Kotov, Dipole-like Electrostatic Asymmetry of Gold Nanorods, Sci. Adv. 4 (2) (2018) e1700682, https://doi.org/10.1126/sciadv.1700682.
[36] X. Huang, S. Neretina, M.A. El-Sayed, Gold Nanorods: from Synthesis and Properties to Biological and Biomedical applications, Adv. Mater. 21 (48) (2009) 4880–4910, https://doi.org/10.1002/adma.200802789.
[37] S.J. Hurst, H.D. Hill, C.A. Mirkin, "Three-Dimensional Hybridization" with Polyvalent Dna–gold Nanoparticle Conjugates, J. Am. Chem. Soc. 130 (36) (2008) 12192–12200, https://doi.org/10.1021/ja804266j.
[38] R. Jin, Y. Charles Cao, E. Hao, G.S. Métraux, G.C. Schatz, C.A. Mirkin, Controlling Anisotropic Nanoparticle Growth through Plasmon Excitation, Nature 425 (6957) (2003) 487–490, https://doi.org/10.1038/nature02020.